Zero Thermal Expansion and Abrupt Amorphization on Compression in Anion Excess ReO_3-type Cubic $YbZrF_7$

John O. Ticknor,[#†] Brett R. Hester,[#] Joshua W. Adkins,[#&] Wenqian Xu,[‡] Andrey A. Yakovenko,[‡] and Angus P. Wilkinson*[,#,§]

[#] School of Chemistry and Biochemistry, Georgia Institute of Technology, Atlanta, GA 30332-0400, United States

[‡] X-ray Science Division, Advanced Photon Source, Argonne National Laboratory, Argonne, Illinois 60439, United States

[§] School of Materials Science and Engineering, Georgia Institute of Technology, Atlanta, GA 30332-0245, United States

ABSTRACT: Heat treatment of cubic $YbZrF_7$, after quenching from 1000 °C, leads to a material displaying precisely zero thermal expansion at ~300 K and negative thermal expansion at lower temperatures. The zero thermal expansion is associated with a minimum in the lattice constant at ~300 K. X-ray total scattering measurements are consistent with a previously proposed model where the incorporation of interstitial fluoride into the ReO_3-related structure leads to both edge and corner sharing coordination polyhedra. The temperature dependence of the experimental pair correlation functions suggest that the expansion of edge and corner sharing links partly compensate for one another, supporting the hypothesis that the deliberate incorporation of excess fluoride into ReO_3-structure materials can be used as a design strategy for controlling thermal expansion. Cubic $YbZrF_7$ has a bulk modulus, K_0, of 55.4(7) GPa and displays pronounced pressure induced softening, K_0' -27.7(6), prior to an abrupt amorphization on compression above 0.95 GPa. The resulting glass shows a single sharp scattering maximum at Q ~ 1.6 $Å^{-1}$.

1. INTRODUCTION

Since a 2010 report that ScF_3 displays strong negative thermal expansion over a very wide temperature range,[1] the expansion characteristics of ReO_3-type fluorides have received considerable attention. The negative thermal expansion of ScF_3 and related materials is attributable to low frequency phonon modes that soften on volume reduction. These vibrations exist as a consequence of the considerable structural flexibility displayed by the ideal cubic ReO_3-type framework and include not only Rigid Unit Modes (RUMs) but other modes involving the transverse displacement of fluoride.[2-3]

Fluorides often display good transparency into the mid-IR, see for example ZBLAN and similar fluoride glass compositions,[4-6] and when electropositive cations with d^0 electron configurations are employed good transmission can extend out into the UV suggesting optical applications. For many potential applications, the dimensional stability associated with zero thermal expansion is particularly desirable. ReO_3-type fluorides are amenable to a wide range of chemical substitutions providing for control of thermal expansion. However, negative and low thermal expansion is only observed for compositions and conditions where the average structure of the material is cubic, rather than a lower symmetry variant associated with cooperative tilting of the MF_6 octahedra. See, for example, the behavior of TiF_3 [7-8] or $CoZrF_6$.[9-10] Strategies that have been explored in an effort to control thermal expansion in cubic ReO_3-type materials include: a) the formation of ScF_3 based solid solutions incorporating one or more metal (III) see, for example, $Sc_{1-x}Y_xF_3$,[11] $Sc_{1-x}Ti_xF_3$,[8] $Sc_{1-x}Al_xF_3$,[12] (Sc/Fe/Ga)F_3,[13-15] b) the replacement of fluoride by oxide to generate compositions such as TaO_2F[16] and NbO_2F,[17] c) the replacement of M(III) by 1:1 combinations of M(II) and M(IV) to generate compositions such as $CaZrF_6$[9] and related materials,[18-20] d) nano-sizing ScF_3[21] and e) the redox based insertion of lithium into interstitial space in compounds such as (Sc/Fe)F_3.[22] There is also a significant body of literature on "anion excess" ReO_3-related fluorides giving M:F ratios of less than 1:3.[23-31] Some of these compounds have been proposed to be cubic ReO_3-type with interstitial fluoride. The presence of such defects in large concentrations is likely to have a significant effect on both the vibrational modes that are present and the thermal expansion of the material, but there is little work examining the incorporation of excess fluoride into ReO_3-type frameworks as a deliberate strategy for controlling thermal expansion. However, there has been a recent report that thermal expansion can be tuned over a wide range by varying composition in the solid solution system $(Sc_{1-x}Zr_x)F_{3+\delta}$.[32] The authors reported evidence for Zr^{3+} in their samples, and both the role and amount of "excess fluoride", δ, was unclear.

In this paper the response of cubic $YbZrF_7$ to both temperature and pressure is examined. This phase has been identified by Poulain and Tofield[26] as having a cubic ReO_3-derived structure with the excess fluoride incorporated as interstitials. The thermodynamically preferred structures of $LnZrF_7$ (Ln – La- Lu, Y) are apparently monoclinic at room temperature.[33-34] However, $LnZrF_7$ (Ln – Er, Tm, Yb, Lu) can be prepared as metastable cubic ReO_3-related materials, providing for isotropic thermal expansion, by quenching from high temperatures.[33]

2. EXPERIMENTAL SECTION

2.1. Sample Preparation. Results for three different samples of cubic $YbZrF_7$ are reported. They were prepared using a pro-

cedure adapted from that of Poulain. YbF_3 (Alfa Aesar) and ZrF_4 (Strem or Sigma Aldrich) were mixed in stoichiometric amounts inside a nitrogen filled glove box. The mixtures were sealed by welding into nickel tubes without exposure to air. The nickel tubes were then sealed inside evacuated fused quartz ampules. The ampules were heated to 1000 °C over a period of a few hours, held at 1000 °C for 48 (Sample A and Sample X) or 72 (Sample F) hours, and then quenched by dropping into water (Sample A) or an ice bath (Sample F and Sample X). A sample of monoclinic $YbZrF_7$ was prepared by a similar procedure. YbF_3 (Strem, 99.99%) and ZrF_4 (Strem, 99.9%), were mixed, ground and then pressed into a pellet. Pieces of the pellet were sealed by arc welding into a nickel tube, which was then sealed in an evacuated fused quartz ampule. The ampule was heated to 450 °C, held at that temperature for 72 hours and then allowed to cool to room temperature.

2.2. Variable Temperature Powder Diffraction Measurements. Synchrotron X-ray powder diffraction data were acquired using beam line 17-BM at the Advanced Photon Source (APS). Samples were sealed, under a dry nitrogen atmosphere, inside Kapton capillary tubes using an epoxy adhesive. For measurements with sample F, the $YbZrF_7$ was mixed with silicon powder, which served both as an internal standard and a diluent to reduce absorption. Data were recorded using x-rays with a wavelength of 0.7295 Å for sample A, and 0.45336 Å for sample F, on a Perkin Elmer amorphous silicon 2D detector. The sample temperature was varied using an Oxford Cryosystems Cryostream. The nominal temperatures indicated by the Cryostream were corrected using a separate run where a thermocouple, packed in sample material, was placed close to the beam position.

2.3. High Pressure Powder Diffraction Measurements. Synchrotron X-ray powder diffraction data were acquired using beam line 17-BM at the APS as the sample pressure was ramped from ambient to ~2.5 GPa. A wavelength of 0.7295 Å was used for these measurements. The cubic $YbZrF_7$ sample, mixed with NaCl as a pressure calibrant, was compressed using a silicone oil medium (Alfa, m.w. 237 $gmol^{-1}$) in a Diacell Bragg-(G) Diamond Anvil Cell equipped with a diaphragm.

2.4. Variable Temperature Total Scattering Measurements. X-ray total scattering data were acquired using beam line 11-ID-B at the APS. Samples were sealed, under a dry nitrogen atmosphere, inside Kapton capillary tubes using an epoxy adhesive. Data were recorded using an x-ray energy of 86.7 KeV, and a sample to detector distance of ~22 cm. The temperature was varied using an Oxford Cryosytems Cryostream, and data were collected every 20 K on heating from 100 to 500 K.

2.5. Analyses of the Powder Diffraction Data. The 2D diffraction data were integrated using GSAS-II.[35] Rietveld analyses were performed using GSAS[36] and its EXPGUI[37] interface. A structural model proposed by Poulain and Tofield[26] for cubic $YbZrF_7$ was used as the starting point for all of the Rietveld fits. These fits were performed with all the atomic coordinates fixed and a single overall thermal parameter. Analyses of the data obtained at high pressure made use of Le Bail fits for the $YbZrF_7$ and a Rietveld fit for the NaCl pressure callibrant. Pressure was determined from the NaCl unit cell volumes using the Birch equation of state.[38]

2.6. Analyses of the X-ray Total Scattering Data. The 2D total scattering data were integrated using GSAS-II[35] using parameters determined from a CeO_2 callibrant. The integrated sample and background patterns were used along with the GSAS-II software to produce F(Q), S(Q), and G(r). A Q_{max} of 20 $Å^{-1}$ was used in the calculation of G(r). Selected peaks in G(r) were fit using Fityk[39] to estimate interatomic separations. A spline interpolation was used to fit the background and Gaussians were used to fit individual peaks. An example fit, illustrating the procedure, is shown in Fig. S1.

3. RESULTS AND DISCUSSION

3.1. Thermal Expansion of Cubic $YbZrF_7$. Poulain and Tofield reported that cubic $YbZrF_7$ can be prepared with either no long range cation order or partial ordering.[26] None of the cubic $YbZrF_7$ samples used in the present work showed any evidence of superlattice peaks indicative of long range Yb/Zr order. The room temperature lattice constants for the present samples were slightly larger (~4.10 versus 4.07 Å) than those previously reported, which might be indicative of some difference in composition.

The variation of until cell volume with temperature for sample A is shown in Fig. 1a along with a representative Rietveld fit in Fig. 1b. The sample was first cooled from room temperature and then heated from a nominal temperature of 100 to 500 K while diffraction data were recorded. On heating, the unit cell volume went through an initial minimum at ~220 K, and then above 300 K it contracted until ~390 K when it began to expand again. The behavior on cooling was similar to that on heating until ~400 K, but at lower temperatures it was clearly different from that observed during the initial heating. On cooling, the sample displayed positive thermal expansion between ~500 and 310 K (α_V ~ +12 ppm K^{-1}, 500 – 350 K), zero thermal expansion at ~310 K, and negative thermal expansion below this temperature (α_V ~ -6 ppm K^{-1}, 250 – 118 K). The presence of a minimum in the lattice constant at ~310 K results in precisely zero thermal expansion at very close to room temperature. The highly significant difference between heating and cooling is either indicative of an experimental problem, or a structural change on heating the sample above ~300 K. As cubic $YbZrF_7$ is a high temperature entropically favored phase recovered to room temperature using a rapid quench, in this case into water at ~295 K, it is reasonable that on slowly heating above the quench temperature the structure could start to relax, likely by the movement of fluoride. It has previously been reported that heating to ~ 660 K is sufficient to enable the diffusion of both fluoride and cations so that transformation to a cation ordered monoclinic phase can begin.[26]

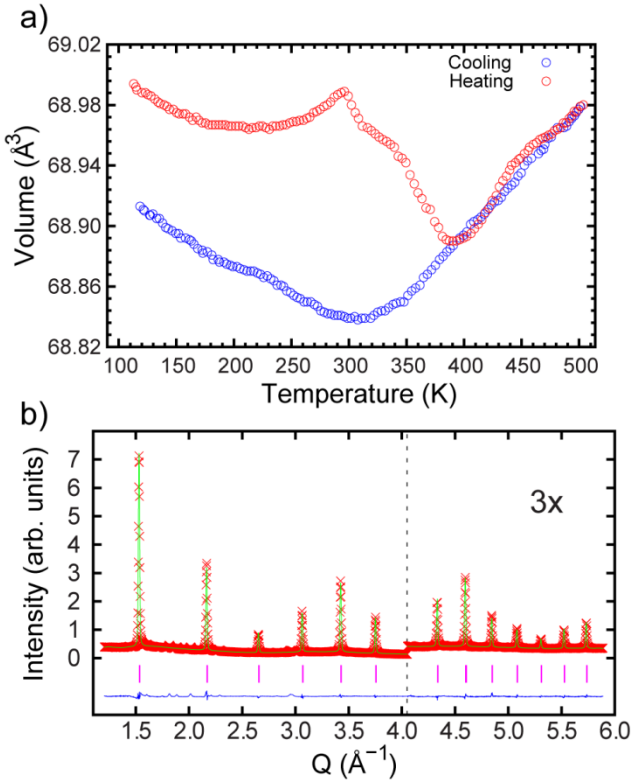

Figure 1. a) Unit cell volume versus temperature for cubic $YbZrF_7$ (sample A) and b) an example Rietveld fit for data taken at ~500 K.

A further variable temperature diffraction measurement was conducted on a different specimen (Sample F), which contained an internal standard (silicon powder) so that any apparent variation in lattice constant with temperature associated with experiment artefacts, such as the sample capillary moving in the x-ray beam, could be distinguished from the intrinsic behavior of the sample. Unit cell volume versus temperature for cubic $YbZrF_7$ (Sample F) and the internal silicon standard are shown in Fig 2a. A representative Rietveld fit to 100 K data for this sample is shown in Figure 2b.

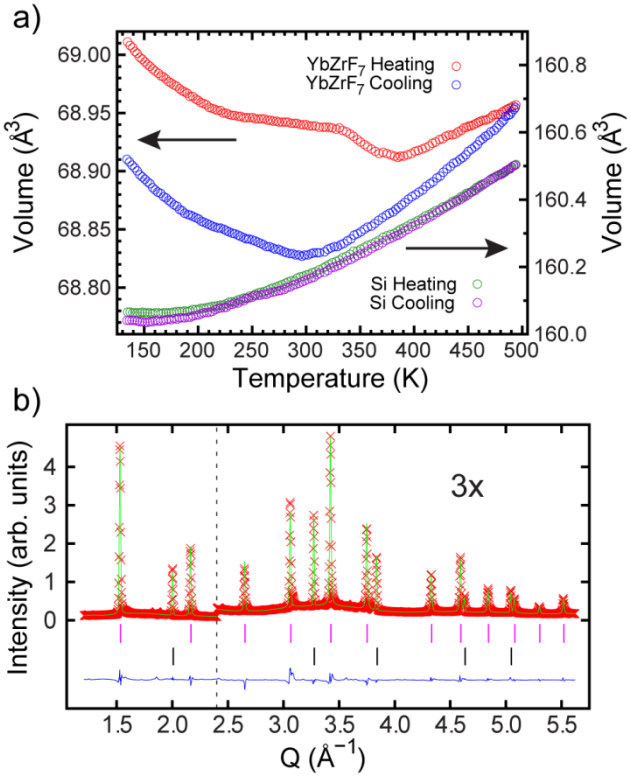

Figure 2. a) Unit cell volume versus temperature for cubic $YbZrF_7$ (sample F) along with the corresponding variation of unit cell volume for the silicon internal standard, and b) a two phase (silicon and cubic $YbZrF_7$) Rietveld fit to data at 100 K.

The thermal expansion displayed by sample F of cubic $YbZrF_7$ is qualitatively the same as that for sample A, but quantitatively different. As the thermal expansion of the silicon internal standard (Fig 2a) reproduces well on heating and cooling, the variation in behavior seen between the first heating and cooling of cubic $YbZrF_7$ must be due to the sample and not an experimental artefact. The quantitative difference between the two samples presumably reflects their differing thermal histories. However, the behavior of both samples on cooling from 500 K is closely related suggesting a similar local structure after the initial heating. It is particularly notable that both samples display zero thermal expansion at very close to 300 K on cooling. Further heating to 500 K or above would presumably lead to additional structural relaxation and different behavior on cooling.

The transition from negative thermal expansion to positive thermal expansion above 300 K for cubic $YbZrF_7$, after first heating to 500 K, is somewhat reminiscent of the behavior observed for ScF_3[1] and $MgZrF_6$.[20] However, in these ideal ReO_3-type materials the change in sign of the expansion occurs at much higher temperatures; ~1100 and ~500 K respectively.

The dependence of expansion on thermal history is both problematic from the perspective of potential applications and, possibly, useful. It is problematic because without precise control of heat treatment it will be hard to achieve reproducible properties, and it is potentially beneficial as by careful heat treatment the temperature at which precisely zero thermal expansion can be achieved is presumably tunable. As some LnZrF7, including YbZrF7,[24] are able to accommodate significant non-stoichiometry while remaining

single phase,[24, 40] the deliberate introduction of non-stoichiometry may also provide for further tuning of the temperature at which zero thermal expansion is achieved. Both the thermal history dependence of expansion in $YbZrF_7$ and the occurrence of precisely zero thermal expansion at close to 300 K are presumably related to the presence of disordered fluoride interstitials in this cubic ReO_3-related material[26] and the response of the associated local structure to temperature.

3.2. Local Structure of Cubic $YbZrF_7$ and its Role in Thermal Expansion. X-ray total scattering data were acquired for cubic $YbZrF_7$ as a function of temperature to gain insight into the local structure of this anion excess ReO_3-type material and its physical properties. The sample used for the total scattering was made separately from those used in the other measurements, but its lattice constant behaved in a similar fashion (Fig. 3a) to that seen for Sample A on first heating from 100 K. The experimental pair distribution function determined from x-ray total scattering data recorded at 100 K is shown in Fig. 3b along with a comparison to that expected for a cation disordered ideal cubic ReO_3-type model "$(Yb,Zr)F_3$" and some of the partial PDFs calculated from this idealized model. This Pm-3m model had 50:50 occupancy of the metal site at (0, 0, 0) and fluoride at (0.5, 0, 0) bridging between the metal positions.

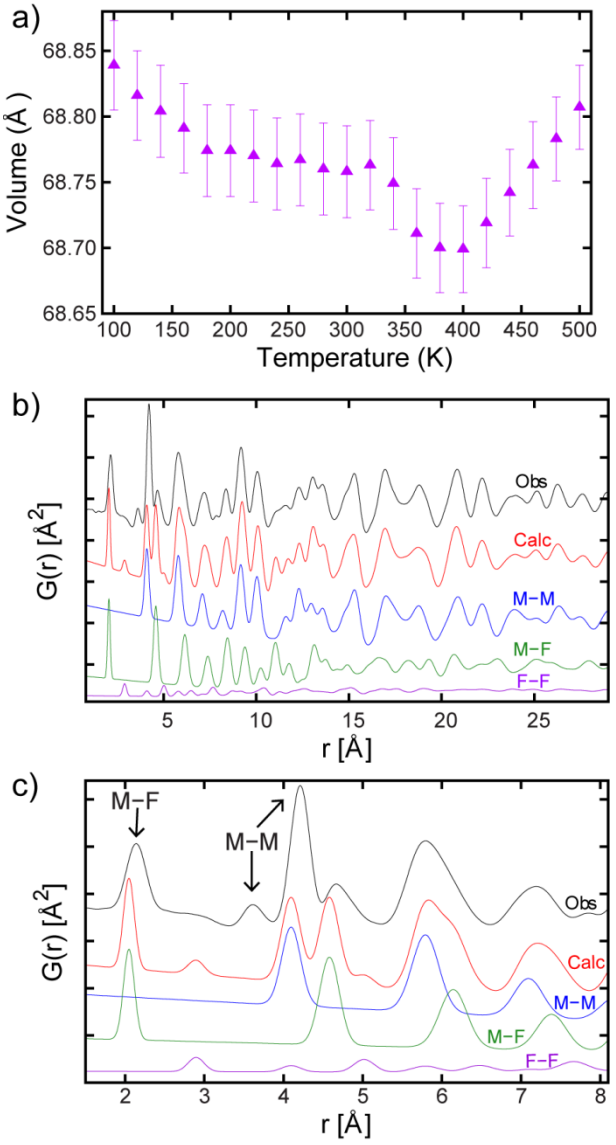

Figure 3. a) Unit cell volume versus temperature derived from Rietveld analyses of the total scattering data for cubic $YbZrF_7$ (Sample X), b) the 100 K experimental pair distribution function compared to an idealized cubic ReO_3-type model and some of the calculated partials, and c) an expanded view of (b).

The experimental PDF shown in Fig 3b is very similar to that calculated from an idealized cubic ReO_3-type model at long distances (r > 14 Å), but it differs from the experimental PDF in several important respects at shorter distances (see Fig 3c). Notably, the first M-F correlation peak in the experimental PDF is at significantly longer average distance (~2.14 Å) than that calculated from the idealized model (~2.05 Å), which is consistent the real material containing bent M-F-M links so that the average M-M separation can be shorter than twice the average M-F distance. Very interestingly, the experimental PDF shows a peak at ~3.63 Å, with no corresponding feature in the PDF calculated from the ideal model. Additionally, the nearest neighbor M-M correlation peak calculated from the model lies at ~4.10 Å, but the corresponding feature in the experimental PDF is at significantly greater distance (4.21 Å). The occurrence of peaks in the experimental PDF at distances both shorted and

longer than that calculated from the idealized model is consistent with the material having two distinct metal – metal nearest neighbor separations.

Based on single crystal x-ray and neutron powder diffraction studies of cation disordered $YbZrF_7$ samples quenched from 1000 °C, Poulain and Tofield[26] proposed a structural model where the average cation coordination number is seven and the material contains both corner sharing and edge sharing polyhedra, which is expected to give rise to two distinct nearest neighbor metal-metal separations. The edge sharing units are generated by replacing single fluoride ions, which in the ideal ReO_3 structure bridge in a corner sharing fashion between metals, with pairs of fluoride ions to form the shared edge between coordination polyhedra (see inset Fig. 4).

The relationship of ordered anion excess ReO_3-type fluoride structures containing edge sharing polyhedra, such as the high temperature (α) and high pressure (γ) forms of ZrF_4, to the ideal ReO_3 structure has recently been discussed in detail by Laval.[31] In the high temperature (α) and high pressure (γ) forms of ZrF_4 the Zr - Zr distances across the shared edges of ZrF_8 polyhedra are much shorter (~3.6 Å) than those between corner sharing polyhedra (4.06 - 4.19 Å).[31, 41] Based on the work of Poulain and Laval, we assign the peak in our exprimental G(r) at ~3.65 Å to metal – metal separations across a shared edge and the peak at ~4.21 Å to a combination of M – M distances associated with corner sharing polyhedra and F – F distances. The assignment of the peak at ~3.65 Å to a M- M separation is supported by the observation that the lattice constant for the sample (~4.10 Å) is less than that of the main M – M correlation peak at ~4.21 Å. These peaks, and the M-F peak at ~2.14 Å, were fit using the program fityk[39] to estimate the changes in average M – F and M- M distances on heating. The results from these fits are shown in Fig. 4.

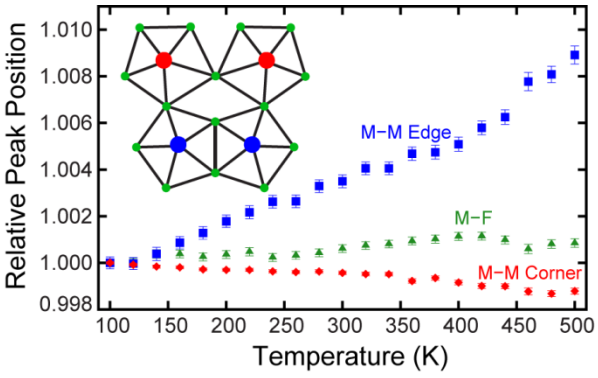

Figure 4. Interatomic separations, as a function of temperature, for cubic $YbZrF_7$ as estimated by fitting individual peaks in the experimental G(r). The average M-F distance (green triangles), M – M distance between polyhedra sharing edges (blue squares) and M – M distances between polyhedra sharing corners (red crosses) have been normalized to their values at 100 K. The error bars are one e.s.d. as estimated by fityk. The inset cartoon represents a possible local structural arrangement.

As expected, the average M – F distance increases on heating until above the temperature at which the variation of lattice constant with temperature (Fig. 3a) suggests the onset of structural relaxation. Interestingly, below this temperature the peak assigned to the average distance between pairs of metals sharing a common polyhedral edge moves to longer distances (α_l ~ 22 ppm K^{-1}) and the peak at ~4.20 Å, assigned as having a major contribution from M – M distances associated with corner sharing units, moves to shorter distance (α_l ~ -3 ppm K^{-1}). This suggests that the response of bridging and corner sharing linkages to increasing temperature can partially compensate one another, potentially leading to low thermal expansion. When comparing these values, it should be noted that there are expected to be 5 times as many corner sharing links as edge sharing ones and that the peak fitting underlying the graphs in Fig. 4 is prone to error from overlapping peaks in the pair correlation function.

3.3. Monoclinic $YbZrF_7$. Annealing cubic $YbZrF_7$ did not provide an efficient route to monoclinic $YbZrF_7$. However, this phase could be readily prepared in pure form from the binary fluorides by heating at 450 °C. Rietveld analyses of lab x-ray diffraction data (see Fig. S2) using a structural model derived from that of $SmZrF_7$ ($P2_1/n$)[34] gave lattice parameters of a = 11.1090(6) Å, b = 5.6377(3) Å, c = 8.8633(5) Å, β = 107.783(3)°.

3.4. Behavior of Cubic $YbZrF_7$ on Compression. The behavior of $YbZrF_7$ was investigated, using a diamond anvil cell (DAC) and synchrotron X-ray diffraction, as the pressure on the sample was continuously increased. The data from these measurements are shown in Fig. 5.

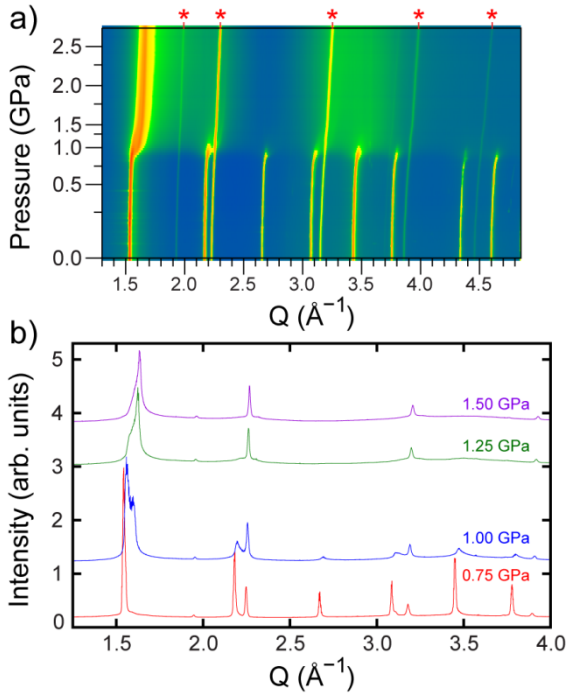

Figure 5. Powder diffraction data as a function of pressure for cubic $YbZrF_7$. (a) General behavior and (b) selected diffraction patterns below, above and close to the observed phase transition. Asterisks mark the positions of peaks from the NaCl pressure marker.

Below ~0.95 GPa $YbZrF_7$ (sample A) maintained its initial cubic structure. Surprisingly, it underwent an abrupt amorphization at ~ 1 GPa with a narrow region of phase coexistence (see Fig. 5b). Cubic ReO_3-type fluorides such as ScF_3[1] and $MgZrF_6$[20] undergo symmetry lowering crystal to crystal transitions on compression, which are associated with the correlated tilting of corner sharing octahedra. In the case of cubic YbZrF7, the presence of disordered

interstitial fluoride may serve to stiffen the framework, by the introduction of edge sharing polyhedra, and stabilize the structure against a phase transition associated with octahedral tilting. At high pressure (> 1.25 GPa) there are no Bragg peaks from the $YbZrF_7$ sample, just a single quite sharp scattering maximum (Q= 1.62 $Å^{-1}$ at 1.25 GPa). We are not aware of any published work on related materials reporting abrupt amorphization on compression. While pressure induced amorphization is common for negative thermal expansion framework materials, the loss of long range structural order usually takes place over an extended pressure range.[42-43] The structural changes underpinning the abrupt amorphization are not clear and warrant further investigation.

The diffraction data for cubic $YbZrF_7$ (0 – 0.93 GPa) were analyzed using the LeBail method (see Fig 6a) to obtain lattice constants versus pressure. A 3rd order Birch-Murnaghan equation of state was fit to the resulting unit cell volumes (Fig. 6b), using the program EosFit7,[44] leading to the following parameters: V_0 = 68.937(5) Å, K_0 = 55.4(7) GPa and K_0' = -27.7(6). The bulk modulus is close to those previously reported for other cubic ReO_3-type fluorides and oxyfluorides: ScF_3, 57(3) GPa;[1] $CaZrF_6$, 42.1(8) GPa;[9] $MgZrF_6$, 48.2(5) GPa;[20] $CaNbF_6$, 33.7(4) GPa;[20] TaO_2F, 36(3) GPa;[45] NbO_2F, 25(1) GPa.[46] While the occurrence of pronounced softening on compression, as seen for $YbZrF_7$ (K_0' = -27.7(6)), is unusual for most materials, it has been predicted[47] and found to be quite common amongst negative thermal expansion solids.[9, 20, 48]

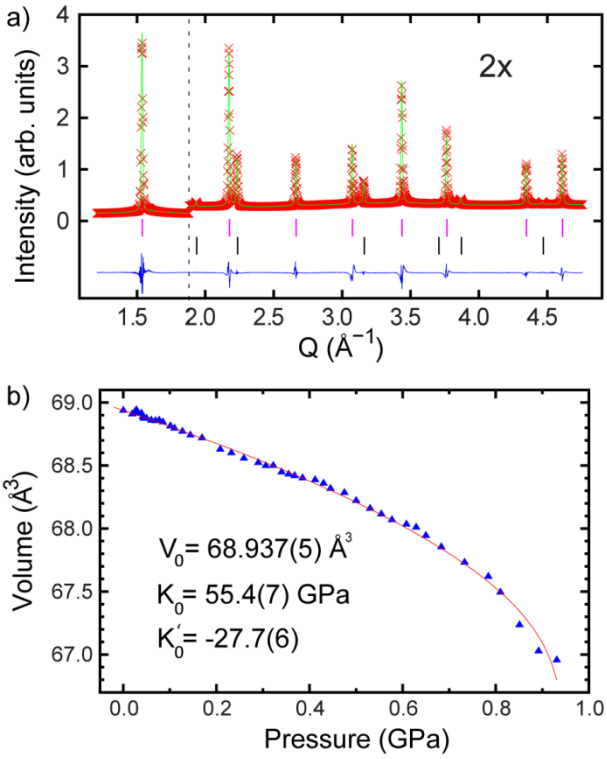

Figure 6. a) A representative fit to the ambient diffraction data for cubic $YbZrF_7$ in a diamond anvil cell, and b) unit cell volume versus pressure fit to a 3rd order Birch-Murnaghan equation of state.

4. CONCLUSIONS

Cubic $YbZrF_7$ samples displaying precisely zero thermal expansion at ~300 K can be prepared by quenching from high temperature followed by heat treatment. However, the thermal expansion behavior of these metastable materials depends on their thermal history. Variable temperature x-ray total scattering suggests that the local structure associated with the presence of interstitial fluoride plays a significant role in the material's thermal expansion, indicating that the deliberate incorporation of excess anions into ReO_3-type fluorides is a viable strategy for the design of controlled thermal expansion solids. On compression below ~0.95 GPa cubic $YbZrF_7$ shows very pronounced pressure induced softening. While unusual for most materials, it has been predicted to be common amongst NTE framework solids.[47] On further compression, the material undergoes an abrupt amorphization, rather than a transition based on the correlated tilting of coordination polyhedral as seen in ideal ReO_3-type fluorides such as ScF_3 and $MgZrF_6$.

ASSOCIATED CONTENT

Supporting Information

The Supporting Information is available free of charge on the ACS Publications website at DOI: XXXXXXX.

Rietveld fit for monoclinic $YbZrF_7$, fit to G(r) for cubic $YbZrF_7$ using fityk, unit cell volume versus temperature, unit cell volume versus pressure, interatomic separations versus temperature as determined from G(r).

AUTHOR INFORMATION

Corresponding Author

* E-mail: angus.wilkinson@chemistry.gatech.edu

ORCID

Angus P. Wilkinson: 0000-0003-2904-400X

Notes

The authors declare no competing financial interest.

Present Addresses

† J.O.T. : Department of Chemistry, University of British Columbia, Vancouver, Canada.

& J.W.A.: Department of Chemistry, Xavier University, New Orleans, Louisiana, USA.

ACKNOWLEDGMENTS

We are grateful to Olaf Borkiewicz for experimental assistance on beam line 11-ID-B of the APS. The activities at Georgia Tech were supported in part under NSF DMR-1607316. This work made use of the Advanced Photon Source, a U.S. Department of Energy (DOE) Office of Science User Facility operated for the DOE Office of Science by Argonne National Laboratory under contract DE-AC02-06CH11357.

REFERENCES

1. Greve, B. K.; Martin, K. L.; Lee, P. L.; Chupas, P. J.; Chapman, K. W.; Wilkinson, A. P., Pronounced Negative Thermal Expansion from a Simple Structure: Cubic ScF_3. *J. Am. Chem. Soc.* **2010,** *132* (44), 15496-15498.

2. Dove, M. T.; Fang, H., Negative Thermal Expansion and Associated Anomalous Physical Properties: Review of the Lattice Dynamics Theoretical Foundation. *Rep. Prog. Phys.* **2016,** *79* (6), 066503.

3. Hu, L.; Chen, J.; Sanson, A.; Wu, H.; Rodriguez, C. G.; Olivi, L.; Ren, Y.; Fan, L. L.; Deng, J. X.; Xing, X. R., New Insights into the Negative Thermal Expansion: Direct Experimental Evidence for the "Guitar-String" Effect in Cubic ScF_3. *J. Am. Chem. Soc.* **2016,** *138* (27), 8320-8323.

4. Poulain, M., Halide Glasses. *J. Non-Cryst. Solids* **1983,** *56* (1–3), 1-14.

5. Poulain, M.; Lucas, J., History of Fluorinated Glasses. *Actual Chim.* **2006**, 117-118.

6. Nazabal, V.; Poulain, M.; Olivier, M.; Pirasteh, P.; Camy, P.; Doualan, J. L.; Guy, S.; Djouama, T.; Boutarfaia, A.; Adam, J. L., Fluoride and Oxyfluoride Glasses for Optical Applications. *J. Fluorine Chem.* **2012,** *134*, 18-23.

7. Kennedy, B. J.; Vogt, T., Powder X-ray Diffraction Study of the Rhombohedral to Cubic Phase Transition in TiF_3. *Mater. Res. Bull.* **2002,** *37* (1), 77-83.

8. Morelock, C. R.; Gallington, L. C.; Wilkinson, A. P., Evolution of Negative Thermal Expansion and Phase Transitions in $Sc_{1-x}Ti_xF_3$. *Chem. Mater.* **2014,** *26* (5), 1936-1940.

9. Hancock, J. C.; Chapman, K. W.; Halder, G. J.; Morelock, C. R.; Kaplan, B. S.; Gallington, L. C.; Bongiorno, A.; Han, C.; Zhou, S.; Wilkinson, A. P., Large Negative Thermal Expansion and Anomalous Behavior on Compression in Cubic ReO_3-type $A^{II}B^{IV}F_6$: $CaZrF_6$ and $CaHfF_6$ *Chem. Mater.* **2015,** *27*, 3912-3918.

10. Rodriguez, V.; Couzi, M.; Tressaud, A.; Grannec, J.; Chaminade, J. P.; Soubeyroux, J. L., Structural Phase-Transition in the Ordered Fluorides $M^{II}ZrF_6$ (M^{II} = Co, Zn).1. Structural Study. *J. Phys. Condens. Matter* **1990,** *2* (36), 7373-7386.

11. Morelock, C. R.; Greve, B. K.; Gallington, L. C.; Chapman, K. W.; Wilkinson, A. P., Negative Thermal Expansion and Compressibility of $Sc_{1-x}Y_xF_3$ ($x < 0.25$). *J. Appl. Phys.* **2013,** *114*, 213501.

12. Morelock, C. R.; Gallington, L. C.; Wilkinson, A. P., Solid Solubility, Phase Transitions, Thermal Expansion, and Compressibility in $Sc_{1-x}Al_xF_3$. *J. Solid State Chem.* **2015,** *222*, 96-102.

13. Hu, L.; Chen, J.; Fan, L.; Ren, Y.; Huang, Q.; Sanson, A.; Jiang, Z.; Zhou, M.; Rong, Y.; Wang, Y.; Deng, J.; Xing, X., High-Curie-Temperature Ferromagnetism in $(Sc,Fe)F_3$ Fluorides and its Dependence on Chemical Valence. *Adv. Mater.* **2015,** *27* (31), 4592-4596.

14. Hu, L.; Chen, J.; Fan, L.; Ren, Y.; Rong, Y.; Pan, Z.; Deng, J.; Yu, R.; Xing, X., Zero Thermal Expansion and Ferromagnetism in Cubic $Sc_{1-x}M_xF_3$ (M = Ga, Fe) over a Wide Temperature Range. *J. Am. Chem. Soc.* **2014,** *136* (39), 13566-13569.

15. Qin, F.; Chen, J.; Aydemir, U.; Sanson, A.; Wang, L.; Pan, Z.; Xu, J.; Sun, C.; Ren, Y.; Deng, J.; Yu, R.; Hu, L.; Snyder, G. J.; Xing, X., Isotropic Zero Thermal Expansion and Local Vibrational Dynamics in $(Sc,Fe)F_3$. *Inorg. Chem.* **2017,** *56*, 10840-10843.

16. Tao, J. Z.; Sleight, A. W., Very Low Thermal Expansion in TaO_2F. *J. Solid State Chem.* **2003,** *173*, 45-48.

17. Wilkinson, A. P.; Josefsberg, R. E.; Gallington, L. C.; Morelock, C. R.; Monaco, C. M., History Dependent Thermal Expansion in "NbO_2F". *J. Solid State Chem.* **2014,** *213*, 38-42.

18. Han, F.; Hu, L.; Liu, Z.; Li, Q.; Wang, T.; Ren, Y.; Deng, J.; Chen, J.; Xing, X., Local structure and controllable thermal expansion in the solid solution (Mn1-xNix)ZrF6. *Inorganic Chemistry Frontiers* **2017**.

19. Hu, L.; Chen, J.; Xu, J.; Wang, N.; Han, F.; Ren, Y.; Pan, Z.; Rong, Y.; Huang, R.; Deng, J.; Li, L.; Xing, X., Atomic Linkage Flexibility Tuned Isotropic Negative, Zero, and Positive Thermal Expansion in $MZrF_6$ (M = Ca, Mn, Fe, Co, Ni, and Zn). *J. Am. Chem. Soc.* **2016,** *138* (44), 14530-14533.

20. Hester, B. R.; Hancock, J. C.; Lapidus, S. H.; Wilkinson, A. P., Composition, Response to Pressure, and Negative Thermal Expansion in $M^{II}B^{IV}F_6$ (M = Ca, Mg; B = Zr, Nb). *Chem. Mater.* **2017,** *29* (2), 823-831.

21. Yang, C.; Tong, P.; Lin, J. C.; Guo, X. G.; Zhang, K.; Wang, M.; Wu, Y.; Lin, S.; Huang, P. C.; Xu, W.; Song, W. H.; Sun, Y. P., Size Effects on Negative Thermal Expansion in Cubic ScF_3. *Appl. Phys. Lett.* **2016,** *109* (2), 023110.

22. Chen, J.; Gao, Q.; Sanson, A.; Jiang, X.; Huang, Q.; Carnera, A.; Rodriguez, C. G.; Olivi, L.; Wang, L.; Hu, L.; Lin, K.; Ren, Y.; Lin, Z.; Wang, C.; Gu, L.; Deng, J.; Attfield, J. P.; Xing, X., Tunable Thermal Expansion in Framework Materials through Redox Intercalation. *Nat. Commun.* **2017,** *8*, 14441.

23. L'Helgoualch, H.; Poulain, M.; Rannou, J. P.; Lucas, J., Nonstoiciometric MY_{2+X} and MY_{3+X} Cubic Phases in the System ZrF_4/CaF_2. *C.R. Hebd. Seances Acad. Sci. Paris Serie C* **1971,** *272* (14), 1321-1324.

24. Poulain, M.; Lucas, J., The System MF_2-ZrF_4 (M=Mg,Mn,Fe,Co,Ni,Zn). The Fluorozirconates of the Cubic Rare Earths. *Rev. Chem. Miner.* **1975,** *12* (1), 9-16.

25. Tofield, B. C.; Poulain, M.; Lucas, J., Nonstoichiometry in anion-excess ReO_3 phases - structure of $Zr_{0.8}Yb_{0.2}F_{3.2}O_{0.3}$ ($MX_{3.5}$) by powder neutron diffraction. *J. Solid State Chem.* **1979,** *27* (2), 163-178.

26. Poulain, M.; Tofield, B. C., The Structure of Cubic $YbZrF_7$. *J. Solid State Chem.* **1981,** *39* (3), 314-328.

27. Grannec, J.; Yacoubi, A.; Fournes, L.; Tressaud, A.; Hagenmuller, P., Nonstoichiometry in the System FeF_3-ZrF_4. *J. Solid State Chem.* **1987,** *70* (2), 323-335.

28. Ruchaud, N.; Grannec, J.; Hagenmuller, P.; Soubeyroux, J. L., A Neutron-Diffraction Study of the Anion-Excess Cubic ReO_3-Type Derived Phase $Fe_{0.80}Zr_{0.20}F_{3.20}$. *J. Alloy Compd.* **1992,** *183*, 263-270.

29. Laval, J. P.; Abaouz, A., Crystal Chemistry of Anion-excess ReO_3-Related Phases: Crystal Structure of β-$PrZr_3F_{15}$. *J. Solid State Chem.* **1992,** *96* (2), 324-331.

30. Laval, J. P.; Abaouz, A., Crystal Chemistry of Anion-excess ReO_3-Related Phases: II. Crystal Structure of $PrZr_2F_{11}$. *J. Solid State Chem.* **1992,** *100* (1), 90-100.

31. Laval, J. P., Crystal Chemistry of Anion-Excess ReO_3-Related Phases. III.(1) Gamma-ZrF_4, a High-Pressure Form of Zirconium Tetrafluoride, and a Comparison of MX_4 Structure Types. *Acta Crystallogr. Sect. C-Struct. Chem.* **2014,** *70*, 742-U44.

32. Wang, T.; Xu, J.; Hu, L.; Wang, W.; Huang, R.; Han, F.; Pan, Z.; Deng, J.; Ren, Y.; Li, L.; Chen, J.; Xing, X., Tunable Thermal Expansion and Magnetism in Zr-Doped ScF_3. *Appl. Phys. Lett.* **2016,** *109* (18), 181901.

33. Poulain, M.; Poulain, M.; Lucas, J., Crystal Structure of $SmZrF_7$. Structural relationship with the ReO_3-type. . *J. Solid State Chem.* **1973,** *8* (2), 132-141.

34. Graudejus, O.; Schrotter, F.; Muller, B. G.; Hoppe, R., On the Crystal Structure of $SmZrF_7$ with an Appendix on $EuSnF_7$ and $YSnF_7$. *Z. Anorg. Allg. Chem.* **1994,** *620* (5), 827-832.

35. Toby, B. H.; Von Dreele, R. B., GSAS-II: The Genesis of a Modern Open-Source All Purpose Crystallography Software Package. *J. Appl. Crystallogr.* **2013,** *46*, 544-549.

36. Larson, A. C.; Von Dreele, R. B., *GSAS - General Structure Analysis System*. Report LA-UR-86-748: Los Alamos Laboratory, 1987.

37. Toby, B. H., EXPGUI, a Graphical User Interface for GSAS. *J. Appl. Crystallogr.* **2001,** *34*, 210-213.

38. Birch, F., Equation of State and Thermodynamic Parameters of Sodium Chloride to 300 kbar in the High-Temperature Domain. *J. Geophys. Res. B* **1986,** *91* (B5), 4949-4954.

39. Wojdyr, M., Fityk: A General-Purpose Peak Fitting Program. *J. Appl. Crystallogr.* **2010,** *43*, 1126-1128.

40. Poulain, M.; Lucas, J., Rare-Earth Fluorozirconates $LnZrF_7$. *Mater. Res. Bull.* **1972,** *7* (4), 319-&.

41. Papiernik, R.; Mercurio, D.; Frit, B., The Structure of Zirconium Tetrafluoride, α-ZrF_4. *Acta Crystallogr. Sect. B: Struct. Sci.* **1982,** *38* (SEP), 2347-2353.

42. Varga, T.; Wilkinson, A. P.; Jupe, A. C.; Lind, C.; Bassett, W. A.; Zha, C.-S., Pressure-Induced Amorphization of Cubic ZrW_2O_8 Studied in-situ and ex-situ by Synchrotron X-ray Absorption Spectroscopy and Diffraction. *Phys. Rev. B* **2005,** *72*, 024117.

43. Wilkinson, A. P.; Greve, B. K.; Ruschman, C. J.; Chapman, K. W.; Chupas, P. J., Pressure Induced Amorphization of $ZrMo_2O_8$ and its

Relaxation on Decompression as Seen by in-situ Total X-ray scattering. *J. Appl. Phys.* **2012,** *112* (2), 023511-6.

44. Gonzalez-Platas, J.; Alvaro, M.; Nestola, F.; Angel, R., EosFit7-GUI: A New Graphical User Interface for Equation of State Calculations, Analyses and Teaching. *J. Appl. Crystallogr.* **2016,** *49* (4), 1377-1382.

45. Cetinkol, M.; Wilkinson, A. P.; Lind, C.; Bassett, W. A.; Zha, C.-S., High-Pressure Powder Diffraction Study of TaO_2F. *J. Phys. Chem. Solids* **2007,** *68*, 611-616.

46. Carlson, S., High-Pressure Studies of the Cubic to Rhombohedral Transformation in NbO_2F. *J. Appl. Crystallogr.* **2000,** *33*, 1175-1176.

47. Fang, H.; Dove, M. T.; Phillips, A. E., Common Origin of Negative Thermal expansion and other Exotic Properties in Ceramic and Hybrid Materials. *Phys. Rev. B* **2014,** *89* (21), 214103.

48. Alabarse, F. G.; Silly, G.; Brubach, J. B.; Roy, P.; Haidoux, A.; Levelut, C.; Bantignies, J. L.; Kohara, S.; Le Floch, S.; Cambon, O.; Haines, J., Anomalous Compressibility and Amorphization in $AlPO_4$-17, the Oxide with the Highest Negative Thermal Expansion. *J. Phys. Chem. C* **2017,** *121* (12), 6852-6863.

Insert Table of Contents artwork here